Effect of Marangoni flow during the solidification of a Fe-0.82wt.%C steel alloy

Journal of Physics: Conference Series **2766** (2024) 012198 doi:10.1088/1742-6596/2766/1/012198

Effect of Marangoni flow during the solidification of a Fe-0.82wt.%C steel alloy

Ibrahim Sari, Menghuai Wu Andreas Ludwig and Abdellah Kharicha

Metallurgy Department, Montanuniversitaet of Leoben, Franz-Josef-Str. 18, A-8700 Leoben, Austria.

E-mail: abdellah.kharicha@unileoben.ac.at

Abstract. A two-phase Mixture model is proposed to simulate the liquid-solid phase transition of a Fe-0.82wt%C steel alloy under the effect of Marangoni flow. This model simplifies computations by solving a single momentum and enthalpy equation for the mixture phase using a three-dimensional finite volume method. The simulation involves solidifying a rectangular ingot ($100 \times 10 \times 100$ mm^3) from the cold bottom surface towards the hot-free surface at the top. To facilitate heat exchange with the surrounding environment, a high heat transfer coefficient of h = 600 W/m^2/K was applied on the bottom surface to establish an upward solidification direction. However, a lower heat transfer coefficient of 20 W/m^2/K was applied on the top free surface, which was considered flat. This study aims to examine the effect of Marangoni flow generated by surface tension on flow and segregation patterns. The results show that the Marangoni flow emerges at the free surface and penetrates into the liquid depth, leading to the formation of hexagonal patterns along the liquid thickness. Upon full solidification, macro-segregation also exhibits hexagonal structures, mirroring the stationary hexagonal shapes generated by Marangoni flow.

1. Introduction

The Rayleigh-Bénard-Marangoni (RBM) convection constitutes a complex fluid dynamics phenomenon that arises in systems subject to temperature gradients and surface tension variations. This intricate convection process combines the classical Rayleigh-Bénard convection and the Marangoni effect, creating dynamic fluid flow patterns and heat transfer characteristics. In a Rayleigh-Bénard-Marangoni system, a vertical temperature gradient leads to the formation of convective cells as a consequence of buoyancy-driven convection. The interaction between temperature differences and surface tension gradients introduces the Marangoni effect, where variations in surface tension across the fluid interface induce flow. Unlike conventional Rayleigh-Bénard convection, where the fluid's properties remain uniform at the free surface, the Marangoni effect introduces additional complexities by allowing temperature-dependent changes in surface tension to influence the flow dynamics. Many researchers [1-6] have conducted numerical and experimental investigations, considering the Rayleigh-Bénard-Marangoni (RBM) convection phenomenon. In a numerical study, Rachid Es Sakhy et al. [7] investigated the Rayleigh-Benard Marangoni (RBM) flow in a cylindrical geometry filled with silicon oil, heated from the bottom and with a free upper surface. This configuration generated a temperature gradient that triggered the formation of convective cells. The authors examined the formation of cells and hexagonal patterns at varying Marangoni and Rayleigh numbers. They found that the appearance of

hexagonal cells was directly linked to the Marangoni number (Ma). Notably, in the absence of surface tension (Ma = 0), no hexagonal patterns were formed. However, at a higher Marangoni number of Ma = 2000, hexagonal cells emerged, and their number increased with increasing Rayleigh number. Additionally, it was reported that the size and number of hexagonal cells augmented with increasing Marangoni number. Rahal et al. [8] conducted an experimental study to investigate the dynamics of Bénard-Marangoni convection in a circular geometry filled with silicone oil. Their findings indicated that the number of cells formed in the fluid decreased as a function of Marangoni number (Ma). This observation suggests that Marangoni forces play a crucial role in pattern formation and dynamics in Bénard-Marangoni convection. Furthermore, the Marangoni flow promotes segregation which is influenced also by the size of the secondary dendrite arm spacing (SDAS) which in turn directly controls the mushy zone permeability and macro-segregation phenomena. The evolution and the final value of SDAS can be predicted based on the cooling rate and the tip radius as described elsewhere [9, 10].

This paper presents a 3D numerical simulation model to investigate the influence of Marangoni flow on the formation of hexagonal structures in terms of flow patterns and the morphology of segregation during the solidification of Fe-0.82wt%C steel alloy. Particular emphasis is placed on regulating both the size and number of hexagonal cells. The fluid movement is driven by two key mechanisms: the buoyancy effect, arising from variations in fluid density caused by temperature and concentration gradients, and the Marangoni-driven flow, driven by surface tension gradients. Therefore, a system of equations will be presented to treat RBM convection phenomena that include the effect of the Marangoni flow on velocity, thermal fields, and the morphology of the segregation structures after the full solidification.

2. Model description

A 3D Two-phase mixture columnar solidification model has been performed to investigate the effect of Marangoni flow on segregation patterns. The two phases refer to the liquid melt (primary phase) and columnar dendrite trunks (secondary phase), and their amounts are quantified by their volume fractions, f_l, and f_s, respectively, their volume fractions sum up to one, denoted as $f_l + f_s = 1$. The columnar phase is stationary, i.e. us = 0; while the motion of the fluid is calculated by solving the momentum conservation equation.

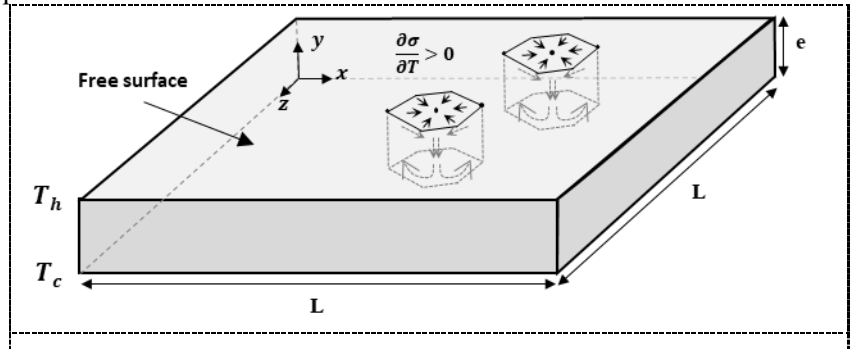

Figure 1. Sketch of the simulated domain.

Except for the conservation of species, which is solved only in the liquid phase. The volume-average conservation equations of mass, momentum, and enthalpy are solved for the mixture phase. The equations are presented in table 1, where ρ_m and um are the mixture density and velocity, respectively. In the present work, the density in the liquid and the solid phases is considered constant $\rho_l = \rho_s$. f denotes the volume fraction, p is the shared pressure, and μ the dynamic viscosity. C_l is the liquid concentration, h is the enthalpy per unit mass, k_{eff} is the effective thermal conductivity, and the subscripts "i" refer to either liquid (l) or solid (s). F_{Darcy}, C_{sl}, and S_T, are the source terms for momentum, species, and enthalpy conservation equations, respectively. $A_{mush} = 10^7$ kg m^{-3} s^{-1} is the mushy zone coefficient, $\epsilon = 10^{-3}$ is an arbitrary constant that is used to avoid dividing by zero. $C_s^* = k\,((T-T_M))/m_l$ is the solid concentration at equilibrium, where k, T, T_M, and ml are the partition coefficient, temperature, melting temperature,

and liquidus slope, respectively, and L is the latent heat of fusion. The thermophysical properties of fe-0.82wt%C alloy are given elsewhere, [11, 12].

Table 1. Volume-average conservation equations.

Mass conservation:	$\frac{\partial \rho_m}{\partial t} + \nabla \cdot \left(\rho_m \vec{u}_m \right) = 0$	(1)
Momentum conservation:	$\frac{\partial \left(\rho_m \vec{u}_m \right)}{\partial t} + \nabla \cdot \left(\rho_m \vec{u}_m \vec{u}_m \right) = -\nabla p + \nabla \left(\rho_m \mu \nabla \vec{u}_m \right) + \rho \vec{g} - \vec{F}_{darcy}$	(2)
Species conservation:	$\frac{\partial \left(\rho_l f_l c_l \right)}{\partial t} + \nabla \cdot \left(\rho_l f_l \vec{u}_l c_l \right) = \nabla \left(\rho_l D_l \nabla c_l \right) + c_{sl}$	(3)
Enthalpy conservation:	$\frac{\partial}{\partial t} \left(\sum_{i=1}^{2} \rho_i f_i c_{pi} T_i \right) + \nabla \cdot \left(\sum_{i=1}^{2} \rho_i f_i \vec{u}_i h_i \right) = \nabla \left(k_{eff} \nabla T \right) + S_T$	(4)

The numerical model was applied to a 3D rectangular geometry (figure. 1) initially filled with molten Fe-0.82wt%C steel alloy. The side surfaces were assumed adiabatic, while the top and bottom surfaces have a hot and cold temperature. The top surface was considered a free surface and has a positive surface tension coefficient, which means that the surface tension increases with temperature. The surface tension created a horizontal non-uniform temperature distribution along the free surface, causing the formation of flow patterns and convective cells known as Marangoni cells as illustrated in figure 1. The model has been described in detail elsewhere [13].

Table 2. Exchange terms used in the conservation equations.

Momentum Transfer:	$\vec{F}_{Darcy} = \frac{f_s^2}{\left(1 - f_s\right)^3 + \varepsilon} A_{mush} \vec{u}_l$	(5)
Species Transfer:	$C_{sl} = -\rho_l \frac{\partial \left(c_s^* f_s \right)}{\partial t}$	(6)
Enthalpy Transfer:	$S_T = \rho_l L \frac{\partial f_s}{\partial t}$	(7)

3. Results and discussion

3.1. Marangoni effect on the flow field

As mentioned previously, the presence of surface tension and temperature gradients leads to the creation of a net force that drives the liquid in the direction of high surface tension known as the Marangoni convection. This phenomenon has a profound impact on the flow patterns on the free surface extending to the liquid depth. The dimensionless number which characterizes the relative effects of surface tension and viscous forces is the Marangoni number (Ma=$\partial\sigma/\partial$T (e DT)/$\mu\alpha$), where, $\partial\sigma/\partial$T is the temperature coefficient of the surface tension. The presence of a Marangoni flow can significantly reorganize the convective cells to perfect hexagonal patterns, as illustrated in figures 1 and 2. The number and the size of the formed cells may change with changing the thermal gradient and the geometry height.

In this part, three simulations were conducted for three cases, each using a different mesh resolution: 1629350 elements for case (a) and 203125 elements for cases (b) and (c). The velocity fields for these cases are presented in figure 2. The height (liquid depth) in cases (a), (b), and (c) was 10, 1.25, and 1.25 mm, respectively, and the thermal gradients were 65, 100, and 65 K, respectively. The length "L" in

case (a) was 10 mm, but in cases (b) and (c) it was 1.25 mm. While all the studied flow situations reached stationary cells, the results were obtained using a transient solver. The results show that the flow patterns exhibited a hexagonal structure due to the influence of surface tension. To investigate the impact of thermal gradient on the flow configuration, figure 2(c) and (b) depict two scenarios with identical aspect ratios but varying thermal gradients (DT = 65 K and 100 K, respectively). In these cases, increasing the thermal gradient from 65 K to 100 K resulted in an increase in the number of convective cells from 15 to 21 (see figure 2). This corresponded to a rise in the Marangoni number from Ma = 1186.8 to 1825.9. The stronger Marangoni force was responsible for the formation of six additional cells and the cells size was noticed to decrease. The temperature coefficient of surface tension was set to $\partial\sigma/\partial T=5\cdot10^{-4}$ N/(m.K) for the case of small thickness (case b and c). The impact of thickness on pattern formation was investigated by examining a larger geometry (8-fold) in case (a) of figure 2. To maintain the same Marangoni number (Ma = 1186.8), the value of $\partial\sigma/\partial T$ was reduced to $6.25\cdot10^{-5}$ N/(m.K) (eight times less) while keeping the thermal gradient constant (DT = 65 K). The results reveal that increasing the thickness to 8-fold resulted in a stable number of cells (15 cells) but dramatically enlarged the cell size. Generally, the number of Marangoni cells increases with increasing Marangoni number. However, when thickness increases while keeping the same Marangoni number, the number of cells remains constant but the cell size grows significantly. The case of e = 1.25 mm was studied in this section (figure 2 (b) and (c)) to explore the influence of thermal gradient and liquid depth on hexagonal pattern formation. However, in subsequent sections, we will focus solely on the geometry with e = 10 mm (as shown in figure 1).

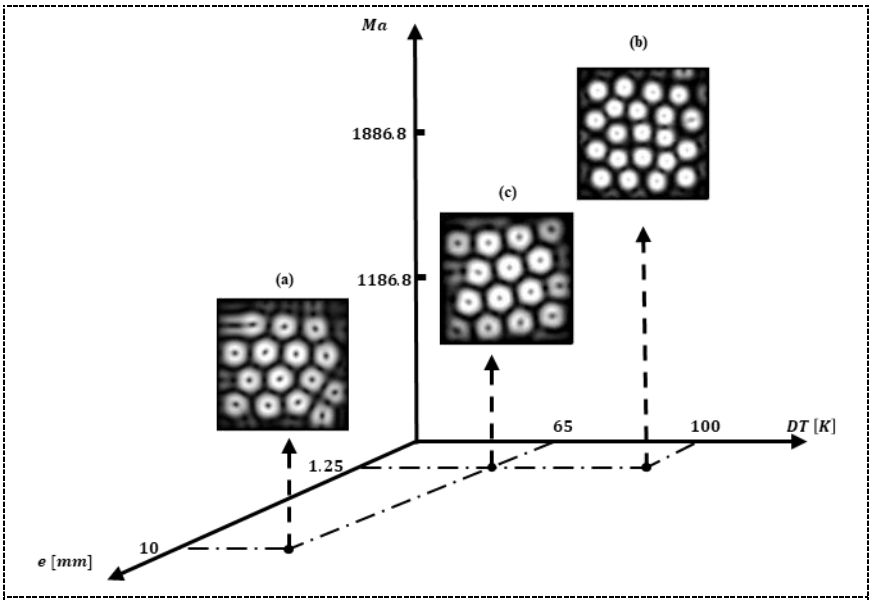

Figure 2. Flow patterns are visualized at e = 0.1 mm for different thermal gradients and different heights.

3.2. Marangoni effect on segregation

Following the formation of hexagonal structures induced by Marangoni effects and surface tension, an intensive heat transfer coefficient (HTC) of h = 600 W/(m² K) was applied to the bottom surface. This HTC facilitated efficient heat extraction between the molten metal and the air, promoting faster growth of columnar structures on the bottom surface compared to other regions. Conversely, a weaker HTC of 20 W/(m² K) was applied along the top free surface. Therefore, solidification starts from the bottom and progresses to the top free surface. After the full solidification of the sample, the segregation which presents the mixture concentration ($C_{mix} = C_l f_l + C_s^* f_s$) was analyzed at different cut planes as shown in figure 3. The results demonstrate that the segregation patterns exhibit hexagonal morphologies, mirroring the influence of Marangoni flow on the segregation structures. The established hexagonal

segregation pattern coincides with the position of the convective cells observed in the previous section (see figure 2(a)).

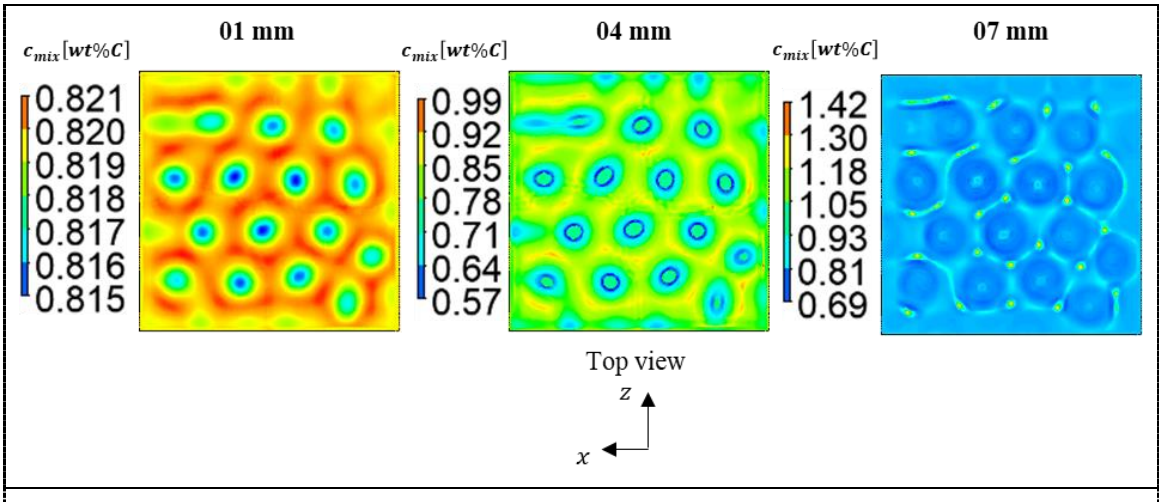

Figure 3. Mixture concentration presented after the full solidification of the sample at 1 mm, 4 mm, and 7 mm presented in left, middle, and right, respectively.

The hexagonal segregation structures presented in figure 3 maintain a consistent position from the bottom to the top. However, the maximum and minimum concentration differences exhibit an increasing trend from the bottom to the top. This behavior is mainly attributed to the strong flow generated at the free surface, which causes a pronounced segregation gradient in the vicinity of this region. However, as the distance between the cut plane and the free surface increases, the Marangoni flow diminishes, leading to a gradual decrease in segregation difference.

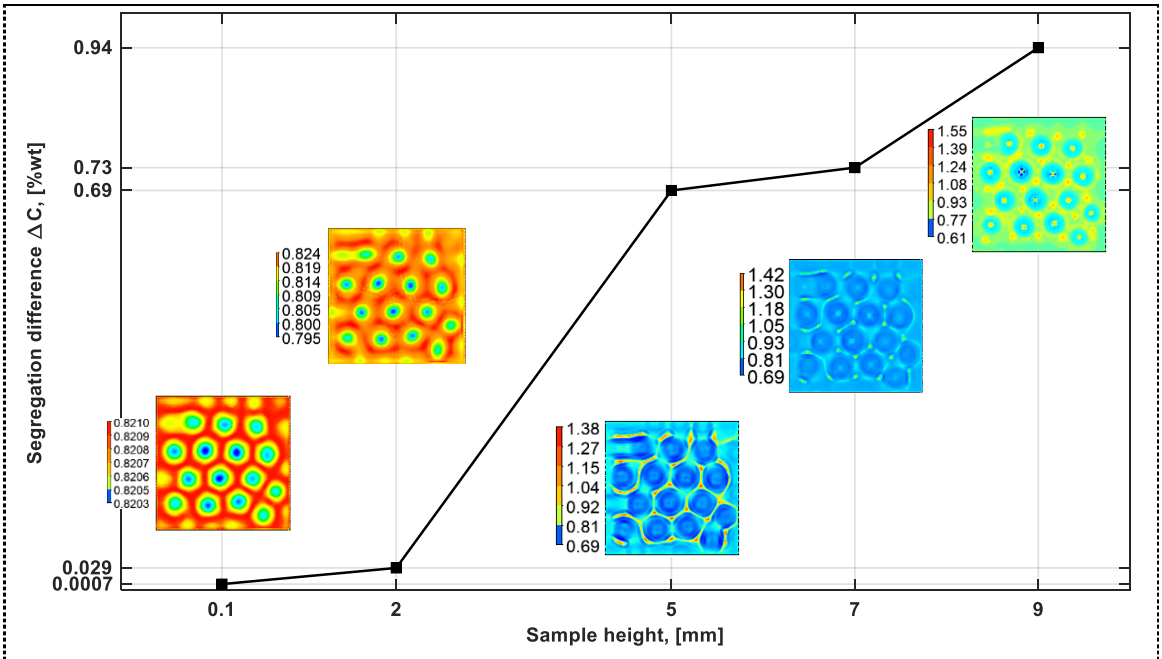

Figure 4. Segregation difference versus the sample thickness. The inset maps are the mixture concentration after the full solidification of the sample at 0.1, 2 mm, 5 mm, 7 mm and 9 mm.

To analyze the segregation difference at different cut planes after the full solidification of the simulated domain, figure 4 presents the segregation difference (ΔC) at 0.1, 2, 5, 7, and 9 mm cut planes. The color bar on the right side of figure 4 aids in comparing the segregation levels at different cut planes, with the minimum and maximum values for each plane being indicated. The results reveal a substantial increase in segregation difference, from $\Delta C = 7.\ 10^{-4}$ to ΔC = 0.94-wt%, between the 0.1 mm cut plane and the 9 mm cut plane. A very weak segregation difference of $7.\ 10^{-4}$ -wt% was observed at e = 0.1 mm, which can be attributed to the weaker flow at the bottom compared to the top, as discussed previously in figure 3 (weaker Marangoni flow at the bottom).

4. Conclusion

A 3D numerical simulation model was developed using the finite volume method to investigate the influence of Marangoni flow induced by surface tension on the solidification of a Fe-0.82wt%C alloy. The aim of this study is to examine the effect of surface tension on the flow and segregation structures. The study revealed that Marangoni flow effectively generates hexagonal convective cells at the free surface, extending throughout the liquid depth. The size and number of hexagonal patterns were found to be related to the thermal gradient and the liquid depth. We found that increasing the thermal gradient resulted in a rise in the number of cells while increasing the geometry height led to larger hexagons. After full solidification, the segregation was found to be in perfect hexagonal shapes, with stronger segregation occurring near the free surface. This study highlights the crucial role of Marangoni flow in producing hexagonal patterns in terms of flow and segregation structures, providing valuable insights for various industrial applications.

References

[1] Chen J J and Lin J D 2000 *Int. J. Heat. Mass. Transf.* **43** 2155-2175
[2] Buffone C, Sefiane K and Easson W 2005 *Phys. Rev. E* **71** 056302
[3] Toussaint G, Bodiguel H, Doumenc F, Guerrier B and C Allain 2008 *Int. J. Heat. Mass. Transf.* **51** 4228-4237
[4] Touazi O, Chenier E, Doumenc F and Guerrier B 2010 *Int. J. Heat. Mass. Transf.* **53** 656-664
[5] Machrafi H, Rednikov A, Colinet P and Dauby P C 2010 *Colloid Interface Sci* **349** 331-353
[6] Medale M and Cerisier P 2015 *Eur. Phys. J. Special Topics* **224** 217-227
[7] Es Sakhy R, El Omari K, Le Guer Y and Blancher S 2014 *Int. J. Therm. Sci.* **86** 198-209
[8] Rahal S, Cerisier P and Azuma H 2007 *Exp Fluids* **43** 547-554
[9] Sari I, Ahmadein M, Ataya S, Hachani L, Zaidat K, Alrasheedi N, Wu M and Kharicha A 2024 *Materials* **17** 865
[10] Sari, I, Alrasheedi N, Ahmadein M, Djuansjah J, Hachani L, Zaidat K, Wu M and Kharicha A 2024 *Materials* **17** 912
[11] Wang W, Luo S and Zhu M 2014 *Comput. Mater. Sci.* **95** 136-148
[12] Luo S, Wang W and Zhu M 2016 *CFD Modeling and Simulation in Materials Processing* (Switzerland) 117-124
[13] Sari I, Wu M, Ahmadein M, Ataya S, Alrasheedi N and Kharicha A 2024 *Materials* **17** 1205